Amorphous Solid Water Films: Transport and Guest−Host Interactions with CO_2 and N_2O Dopants

G. Kumi, S. Malyk, S. Hawkins, H. Reisler,* and C. Wittig*

Department of Chemistry, University of Southern California, Los Angeles, California 90089

Received: August 22, 2005; In Final Form: December 12, 2005

Guest−host interactions have been examined experimentally for amorphous solid water (ASW) films doped with CO_2 or N_2O. The main diagnostics are Fourier transform infrared (FTIR) spectroscopy and temperature programmed desorption (TPD). ASW films deposited at 90 K are exposed to a dopant, and the first molecules that attach to a film enter its bulk until it is saturated with them. Subsequent dopant adsorption results in crystal growth atop the ASW film. There are distinct spectral signatures for these two cases: LO and TO vibrational modes for the crystal overlayer, and an easily distinguished peak for dopant molecules that reside within the ASW film. Above 105 K, the dopant surface layer desorbs fully. Some dopants residing within the ASW film remain until 155 K, at which point the ASW-to-crystalline-ice transition occurs, expelling essentially all of the dopant. No substantial differences are observed for CO_2 versus N_2O. It is shown that annealing an ASW film to 130 K lowers the film's capacity to include dopants by a factor of ∼3, despite the fact that the ASW spectral feature centered at ∼3250 cm^{-1} shows no discernible change. Sandwiches were prepared: ASW−dopant−ASW etc., with the dopant layer displaying crystallinity. Raising these samples past 105 K resulted in the expulsion of essentially all of the crystalline dopant. What remained displayed the same spectral signature as the molecules that entered the bulk following adsorption at the surface. It is concluded that the adsorption sites, though prepared differently, have a lot in common. Dangling OH bonds were observed. When they interacted with a dopant, they underwent a red shift of ∼50 cm^{-1}. This is in qualitative agreement with studies that have been carried out with weakly bound binary complexes. As a result of this study, a fairly complete, albeit qualitative, picture is in place for the adsorption, binding, and transport of CO_2 and N_2O in ASW films.

1. Introduction

Understanding interactions between molecules and ice has been and remains the focus of numerous experimental and theoretical studies, and the dependence of physical properties on structure makes the determination of ice structures a prerequisite for such research. At low temperatures, water can exist in a number of phases. Of these, amorphous and cubic ices lend themselves readily to ultrahigh vacuum studies, and consequently a considerable amount of research involving these forms has been carried out.

Amorphous ice, commonly referred to as amorphous solid water (ASW), is a metastable form of ice. It is the most abundant phase of water in interstellar clouds.[1,2] There is, however, little quantitative agreement among the many published results detailing its physical properties. For example, specific surface areas have been reported that range from ∼12 to 640 $m^2\ g^{-1}$,[3−5] and the temperatures that are required for the rapid (i.e., within 20 min) conversion of ASW to cubic ice vary by more than 20 K.[6−8]

Recent results by Kimmel et al. show that such disagreements may arise from differences in ice preparation.[3] Their investigations indicated that ASW film morphology depends on both the growth conditions and the thermal histories of the films. Accordingly, meaningful comparisons between ASW studies performed by different groups require clear specification of these parameters.

The IR spectrum of ASW does not appear to be a good indicator of film structure. Despite the fact that different preparation conditions lead to ASW samples having a number of different physical properties, spectra obtained at different temperatures and by various investigators have displayed remarkably similar shapes.[9,10] Thus, these spectra are poor diagnostics. In the 2000−4000 cm^{-1} region, ASW spectra are dominated by a broad band that is ∼300 cm^{-1} wide and centered at ∼3250 cm^{-1}. A relatively weak feature at 3696 cm^{-1} is believed to originate from dangling OH, hereafter referred to as *d*-OH groups.[5,11] These groups do not participate in the hydrogen-bonding network present in ice, which is why the *d*-OH line width is relatively narrow. The broad nature of the main spectral signature makes it difficult to discern subtle changes that occur in this band when ASW interacts with added molecular species. Consequently, the properties of the weak *d*-OH band are often monitored to glean information about such interactions and to explore structural changes induced by annealing.

To circumvent problems that derive from the use of a relatively weak signal as the observable, some studies have exploited IR spectral signatures of probe molecules.[12−16] If these molecules interact weakly with water molecules in the ice film, they may serve as good probes of certain properties. From a spectroscopic standpoint, a good probe should possess certain characteristics: an IR band having a narrow line width (to allow small shifts to be easily discerned), and reasonable oscillator strength to facilitate detection. For example, CO and CF_4 have been used as spectral probes of ice morphology because they fit the above criteria.[12,13,16]

10.1021/jp058234y CCC: $33.50
Published on Web 01/26/2006

As probe molecules, both CO_2 and N_2O possess desirable characteristics. For example, in the gas phase, they are stronger absorbers than CO by 1 order of magnitude. It is unclear, however, if the presence of CO_2 or N_2O leads to alterations in ice structure. Sandford and Allamandola report the binding energy of CO to water to be about one-fifth of the energy that binds a water molecule to a water film (~0.5 eV).[17] Thus, it is reasonable to expect that the presence of CO molecules will not lead to significant changes in ice morphology. In contrast, binding energies of around 0.2 eV have been determined for CO_2 desorbing from ice films,[17,18] and therefore interactions between CO_2 and ice might (conceivably) alter ice structure. Though a literature search did not find binding energies of N_2O to ice, they are expected to be similar to those of CO_2.

The study reported here explored the uptake and desorption of CO_2 and N_2O from ASW films by using IR spectroscopy as the main diagnostic. The similar physical properties of CO_2 and N_2O suggested that results obtained with each would be complementary. The observations reported below show that, regardless of the CO_2−ice and N_2O−ice interaction strengths, some spectroscopic characteristics exhibited by CO_2 and N_2O are indeed sensitive to ice morphology. Thus, these molecules can be used to monitor or probe structural changes within the ice film.

The *d*-OH band shifts observed in each probe-ASW system are also reported. Silva and Devlin used these shifts to estimate binding energies of certain molecules to amorphous ice.[15] Recent theoretical results, however, suggest that there is no direct correlation between interaction energy and the magnitude of the *d*-OH band shift. Manca et al. state that these shifts appear instead to be correlated to the local electric field along the OH bond of a dangling OH group.[19] The *d*-OH band shifts induced by CO_2 and N_2O provide yet another experimental test of theoretical models that attempt to elucidate the physical processes responsible for the *d*-OH vibrational frequency. Moreover, the small sizes of CO_2 and N_2O should facilitate their inclusion into quantum mechanical models.

2. Experiment

The experiments were carried out in an ultrahigh vacuum (UHV) chamber (base pressure ~10^{-10} Torr) that was designed to facilitate transmission Fourier transform infrared (FTIR) spectroscopic studies. The arrangement shown in Figure 1 has been discussed in detail elsewhere and will be outlined briefly here.[20] Infrared radiation from the FTIR spectrometer (Nicolet Protegé 460) entered and exited the chamber via calcium fluoride windows. This beam was focused onto the crystal sample and, upon exiting the chamber, onto a liquid nitrogen cooled InSb detector. The beam diameter at the surface was ~8 mm. An air-dryer/CO_2 removal unit (Whatman) purged the entire beam path outside the chamber.

A single crystal sample (approximately 1 mm × 10 mm × 10 mm) was prepared under dry nitrogen conditions and quickly inserted into the chamber. The procedure involved cleaving a MgO(100) crystal (Markatech) twice, creating fresh (100) surfaces at each face. After thoroughly baking the chamber, the sample was annealed at 400 K for 20 min in 10^{-7} Torr of O_2 to minimize oxygen vacancies and removes contaminants.[21] A *k*-type thermocouple was fixed to one edge of the crystal with a high-temperature ceramic adhesive (Aremco 569), while an ion gauge, calibrated for nitrogen, recorded pressure.

The surface holder differed slightly from the one used in our previous FTIR and TPD studies. This change derived from efforts to enhance sample cooling and reduce thermal gradients

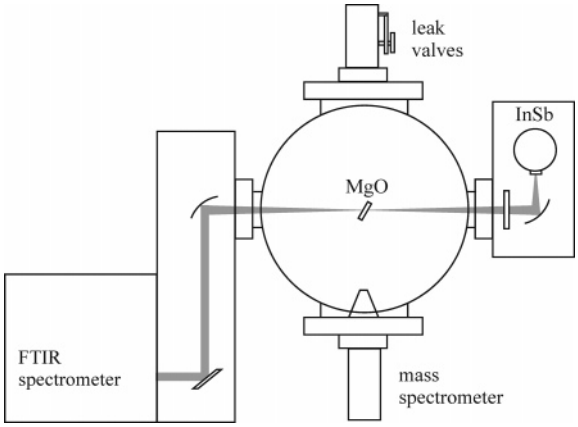

Figure 1. Schematic drawing of the experimental arrangement. IR radiation is reflected from a flat mirror and a focusing mirror (150 mm focal length) before entering the UHV chamber through a CaF_2 window. It passes through the rotatable MgO(100) crystal with a diameter of ~8 mm and exits the chamber through a CaF_2 window. It passes through a wire grid polarizer and is focused (45 mm focal length) onto a 2 mm diameter InSb detector element. The path is purged to remove atmospheric water and carbon dioxide. Precision leak valves dose water and CO_2 or N_2O, and a residual gas analyzer with a narrow aperture observes molecules desorbed from the surface via TPD.

across the surface. The sample was sandwiched between two pairs of copper plates situated at opposite edges of the sample face; i.e., each set sandwiched one edge. Stainless steel screws held the plates together and ensured firm contact between these plates and the sample. One plate of each pair was simply an extension of a copper piece attached to, but electrically isolated from, a liquid nitrogen reservoir. The sample was resistively heated using two tantalum wires tightly held to the edges of the crystal face by the aforementioned pairs of copper plates. Bubbling helium gas through liquid nitrogen in the reservoir, as reported by Xu et al.,[22] kept the reservoir at temperatures below that of liquid nitrogen and lowered the minimum achievable surface temperature by about 10 K. A precision manipulator, to which the reservoir was attached, provided *XYZ* translation and 360° rotation.

Using this arrangement, a surface temperature of 90 K (i.e., approximately 20 K lower than the minimum sample temperature that could be achieved with the previous sample holder) was routine. The importance of this 90 K minimum temperature cannot be overstated, as maintaining temperatures less than 100 K is crucial to the formation of stable N_2O and CO_2 films. Namely, maintaining suitable concentrations of these molecules on a water or MgO(100) surface for the 5−10 min needed to record FTIR spectra required temperatures below 100 K.

Unfortunately, the superior thermal contact between the sample and cooling system in this configuration limited the *maximum* achievable surface temperatures to ~400 and 200 K, with samples at room temperature and 90 K, respectively. In addition, the close proximity of the surface holder components to the sample made it difficult to determine the origin of desorbing molecules during temperature programmed desorption (TPD). Thus, the ability to perform accurate and meaningful TPD was sacrificed when using this new surface holder.

Purified and deionized H_2O was introduced into the chamber via a leak valve following several freeze−pump−thaw cycles. N_2O (Praxair, 99.999%) and CO_2 (Gilmore Liquid Air Co., 99.99%) were dosed through a separate leak valve. In all of the experiments, the admitted gases were background dosed, thereby subjecting both faces of the crystal to the gas, with continuous pumping during dosing.

Each spectrum consisted of an average of 200−500 scans obtained within 5−10 min and recorded with 1 cm^{-1} resolution. A cooled surface, flashed to 400 K just before cooling, served as a reference, i.e., the background traces. The InSb detector cutoff frequency of ∼1850 cm^{-1} set the lower limit on the observable frequency range.

Water coverages were obtained by exposing the MgO(100) surface to a constant flux of water vapor for a fixed period of time prior to recording sample spectra. Thickness was estimated by comparing a water film's integrated absorbance with the integrated absorbance of a water monolayer on MgO(100). Water monolayer coverage was determined using TPD.[20] The adsorbate surface residence time τ can be estimated by using

$$\tau = \tau_0 e^{\Delta H_{ad}/RT_s} \quad (1)$$

where τ_0 typically is assumed to be 10^{-13} s, T_s is the surface temperature, and ΔH_{ad} is the heat of adsorption.[23] The isosteric heat of adsorption of the water monolayer on MgO(100) and the desorption barrier for water molecules on ice are roughly 0.8 and 0.5 eV, respectively.[6,24] At a surface temperature of 100 K, both the monolayer and multilayer films are stable for several hours because of long residence times.

The introduction of N_2O and CO_2 was achieved by exposing water films (and in some cases the MgO(100) substrate) to a background pressure of N_2O or CO_2 for fixed times prior to recording spectra. All probe molecule depositions were performed at 90 K. Ideally, the amount of probe molecules on or within the water film can be estimated by dividing the integrated absorbance of a specific probe IR feature with the integrated absorbance of that same IR feature at monolayer coverage. However, TPD coverage calibrations for these molecules could not be performed because the surface holder suitable for TPD experiments failed to reach temperatures low enough (i.e., <100 K) for a detectable accumulation of these molecules on the MgO(100) surface. Consequently, the background pressure and exposure time for each N_2O and CO_2 dose will be stated. The integrated absorbance of a particular probe molecule IR feature (e.g., the asymmetric stretch band) obtained immediately after dosing N_2O or CO_2 onto the MgO(100) substrate at 90 K was approximately proportional to the exposure time at a constant background pressure.

CO_2 has three active IR bands in the 2000−4000 cm^{-1} region,[25] the most intense being the asymmetric stretch ν_3 fundamental near 2349 cm^{-1}. Studies of CO_2 thin films show that this mode splits into the longitudinal optical (LO) and the transverse optical (TO) modes in crystalline CO_2.[26] The same type of splitting occurs with the ν_3 fundamental mode of crystalline N_2O.[26] The transition dipole moment associated with the LO mode lies perpendicular to the face of the film, and the TO mode transition dipole moment is parallel to the film surface. Consequently, to observe both modes requires incident radiation capable of exciting transition dipole moments perpendicular and parallel to the film surface. As p-polarized light meets this criterion, it was used for most the experiments. For these polarization studies, a wire grid polarizer (Molectron) was placed in the infrared beam path; the angle between the surface normal and incident beam ranged from 48° to 58°.

3. Results

The deposition of water onto a surface whose temperature is less than 130 K results in the formation of a film of amorphous solid water (ASW). The morphology of this film depends on several factors: deposition temperature; water vapor flux, including its angular distribution with respect to the supporting substrate; and the annealing temperature, should there be one.[3] Conversion to crystalline (cubic) ice commences at temperatures around 155 K. Increasing the temperature further results in desorption of all of the multilayer molecules, which is complete by 190 K. Publications reporting IR spectra of these two phases are legion.[7,10,19,20] They reveal that differences exist in the respective IR absorption bands near 3200 cm^{-1}. The current study has used the spectral signatures of N_2O and CO_2 to probe their interactions with thin (i.e., <1000 layers) ASW and cubic ice films.

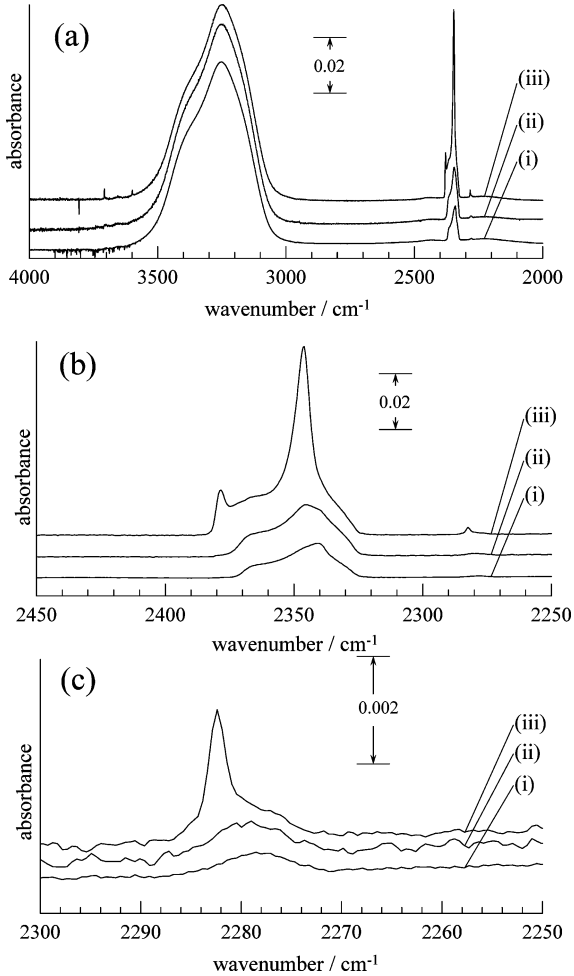

Figure 2. Spectra recorded with p-polarization. (a) Varying amounts of CO_2 were deposited at 90 K onto ASW films of approximately constant thickness (∼65 layers). Exposure to CO_2 was carried out at a pressure of 4×10^{-8} Torr for durations of (i) 1.5 min, (ii) 3 min, and (iii) 6 min. The broad water feature centered at ∼3250 cm^{-1} provides estimates of relative film thicknesses, which are approximately the same for (i)−(iii). (b) The horizontal scale is expanded to emphasize the CO_2 ν_3 region. (c) The horizontal scale is expanded to emphasize the $^{13}CO_2$ ν_3 region.

Interactions of CO_2 with ASW Films. The overall shapes of the absorption spectra obtained after depositing CO_2 onto ASW films at 90 K depend on the amount of CO_2 deposited and the ASW film thickness. Figure 2 shows the trend observed in the ν_3 region upon depositing varying amounts of CO_2 on ASW films of constant thickness. A single band (2325−2375 cm^{-1}) was observed with small doses, with peaks at 2379 and 2345 cm^{-1} evident with higher doses. At 90 K, equal exposures of CO_2 to ASW films that differed only in thickness revealed that the thinner the ASW film the greater the intensities of the features at 2345 and 2379 cm^{-1} (Figure 3).

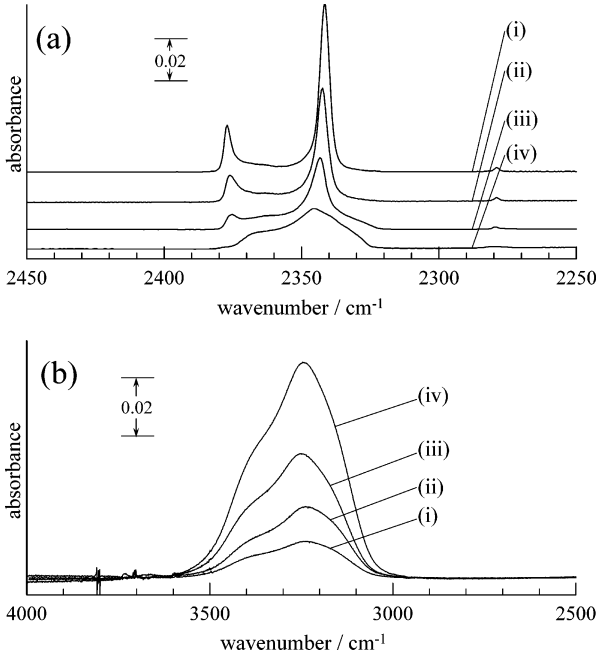

Figure 3. Spectra recorded with p-polarization. The same amount of CO_2 was deposited at 90 K onto ASW films of varying thickness. The films were exposed to CO_2 at 4×10^{-8} Torr for 3 min. H_2O exposure times at 5×10^{-8} Torr for (i)−(iv) were 2, 4, 8, and 16 min, corresponding to 10, 20, 40, and 80 layers, respectively. Entries (a) and (b) show spectral regions for CO_2 and H_2O ν_3, respectively.

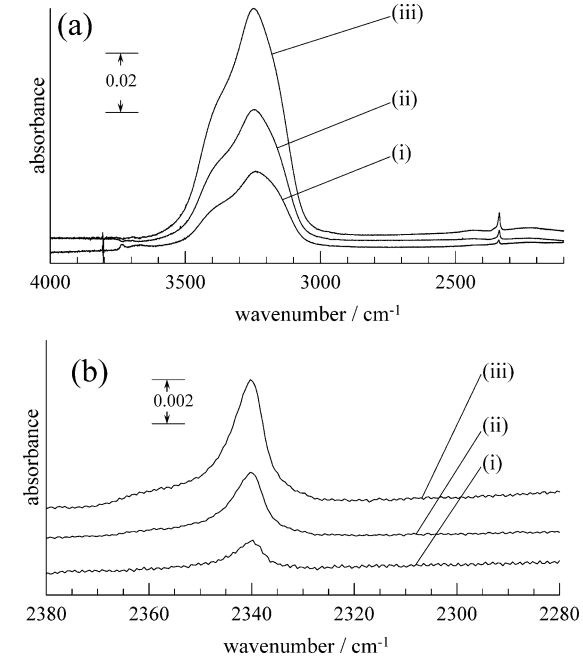

Figure 4. Spectra recorded with p-polarization of the CO_2 that remained after depositing at 90 K equal amounts of CO_2 (3 min at 4×10^{-8} Torr) onto ASW films of varying thickness followed by raising the temperature. The temperature was raised to 105 K where it was held for 15−20 min before each trace was obtained. Entries (i)−(iii) correspond to ASW films of thickness 20, 40, and 80 layers, respectively. Panels (a) and (b) show the same traces on different horizontal scales.

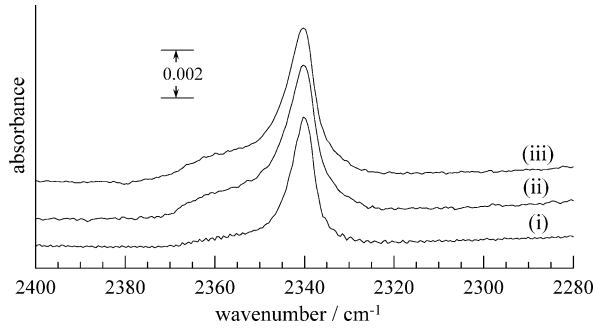

Figure 5. Spectra recorded with p-polarization of the CO_2 that remained after depositing at 90 K different amounts of CO_2 onto ASW films of constant thickness (∼65 layers) and then increasing the temperature to 105 K. The spectra were recorded at 105 K, 15−20 min after the temperature reached 105 K. The CO_2 exposure times at 4×10^{-8} Torr were (i) 1.5, (ii) 3, and (iii) 6 min. See Figure 2 for spectra recorded following CO_2 deposition at 90 K.

Referring to Figure 2, a band was also observed in the $^{13}CO_2$ ν_3 region. It consisted of a peak at about 2278 cm^{-1} at low dosage, and a relatively narrow feature at ∼2282 cm^{-1} that emerged as the amount of accumulated CO_2 increased (Figure 2c). The overall shape of this isotopomer feature depended on both the amount of CO_2 deposited and the ASW thickness. For equal amounts of CO_2 dosed at 90 K, the thinner the ASW film the greater the intensity of the feature at ∼2282 cm^{-1}. The two small peaks on the high-frequency side of the water IR band are CO_2 combination bands (see Figure 2a, trace iii).

Raising the substrate temperature to 105 K for 15−20 min after CO_2 deposition onto an ASW film resulted in a residual CO_2 band around 2340 cm^{-1}. The temperature of 105 K was chosen because experiments involving CO_2 films adsorbed at 90 K on the MgO(100) substrate showed complete CO_2 desorption by 105 K. Both the maximum peak intensity and the integrated absorbance of the residual band were, to within experimental uncertainty, proportional to the ASW film thickness (Figure 4). For ASW films having the same thickness, however, increasing the CO_2 dosage time at 90 K did not necessarily result in a concomitant increase in the integrated absorbance of the 2340 cm^{-1} band (Figure 5). In fact, the 2340 cm^{-1} feature appeared to saturate. Namely, for sufficiently long exposure times, the shape and intensity of this band did not continue to increase with exposure. This behavior is expected when the amorphous host has taken up the maximum amount of CO_2 that it is capable of absorbing

The residual CO_2 band was relatively stable up to the phase transition temperature. During the conversion of ASW to cubic ice, the intensity of this band went almost to zero (Figure 6). A similar phenomenon involving the release of molecules trapped in porous ice films has been reported previously.[27]

It was found that the residual band intensity is sensitive to the amount of water deposited on the CO_2 at 90 K. In a series of "sandwiching" experiments, a fixed amount of CO_2 was deposited between two ASW films. This involved forming the bottom ASW layer, dosing CO_2, and then depositing the top ASW layer. The dosing times for the two ASW layers were chosen in a manner that ensured that the total amount of water in each sandwich remained constant. The results revealed that the thicker was the ASW film on top of the accumulated CO_2, the greater was the intensity of the residual CO_2 peak. Similar sandwiching experiments could not be performed with crystalline ice films because formation of the top cubic ice film would require deposition or annealing temperatures greater than 150 K, and CO_2 desorption begins well below 150 K.

The $^{13}CO_2$ ν_3 region showed no discernible IR signature after 105 K isothermal desorption. This was most likely due to the relatively small percentage of these isotopomers in the CO_2 sample and the small total amount of CO_2 remaining after desorption. Naturally, increasing the total amount of CO_2

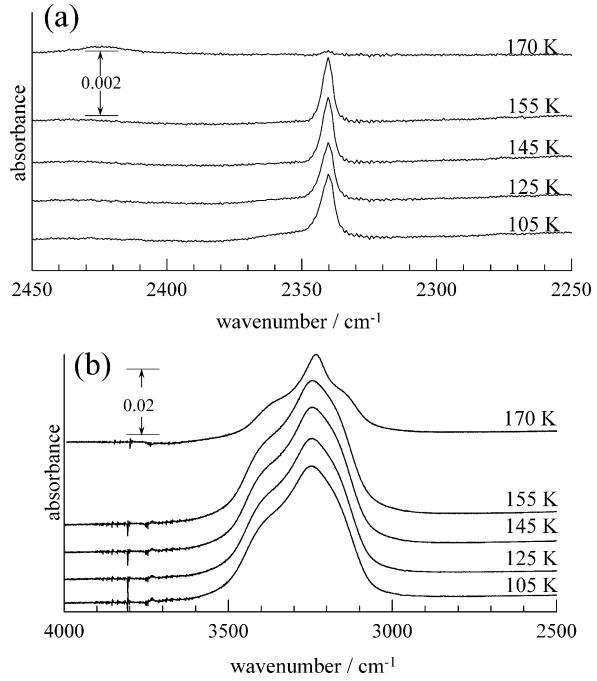

Figure 6. CO_2 was deposited (4×10^{-8} Torr for 4 min) onto a 90 K ASW film of 40 layers. The temperature was then raised to 105 K and held there for 15 min, at which time a spectrum was recorded. The figure depicts the evolution of the spectra as the temperature was increased in steps to those shown and held at these temperatures for the duration of a scan (~8 min). The spectra were recorded immediately after each temperature increase and at the temperatures indicated. Entries (a) and (b) show spectral regions for CO_2 and H_2O, respectively.

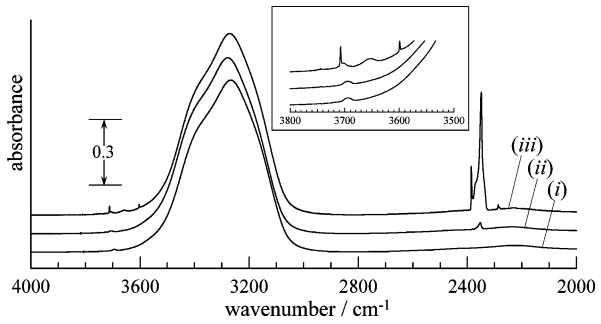

Figure 7. Different amounts of CO_2 were deposited on an ASW film of ~1000 layers at 90 K. The amount of CO_2 was increased via the sequence: (i) no deposition; (ii) 4×10^{-8} Torr for 2 min; (iii) 1×10^{-7} Torr for 16 min. Spectra were recorded immediately following each deposition. The insert shows that the *d*-OH feature is red shifted as a consequence of CO_2 deposition; namely, the small *d*-OH humplet at ~3700 cm^{-1} moves to ~3650 cm^{-1}.

remaining at 105 K by increasing film thickness should eventually lead to a distinguishable signature in the isotopomer ν_3 region.

Converting the ASW film to cubic ice via flash-annealing to 170 K prior to CO_2 deposition drastically altered the outcome of isothermal desorption at 105 K. Though cubic ice films were cooled to 90 K before CO_2 adsorption, no CO_2 spectral features remained after 105 K desorption. Changing the thickness of the cubic film and the CO_2 dosing time did not alter this result.

Experiments monitoring the *d*-OH feature utilized ASW films that were more than 800 layers thick. This stemmed from the difficulty associated with observing the *d*-OH IR band in thinner films (cf., Figures 6 and 7). The spectra presented in Figure 7 were taken between successive doses of CO_2. Each CO_2 deposition added to previously accumulated CO_2 and a new feature (~3655 cm^{-1}) emerged as the amount of CO_2 increased.

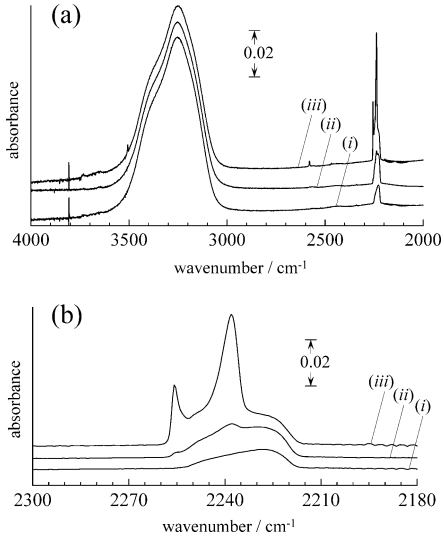

Figure 8. Spectra recorded with p-polarization. (a) Varying amounts of N_2O were deposited onto 90 K ASW films. The broad water feature centered at ~3250 cm^{-1} provides estimates of the relative film thicknesses, which were approximately equal at 70 layers. The N_2O exposure times at 4×10^{-8} Torr were (i) 2 min, (ii) 4 min, and (iii) 8 min. (b) The horizontal scale is expanded to emphasize the N_2O ν_3 region.

Though CO_2 combination bands (3708 and 3599 cm^{-1}) complicate the overall picture, the 3655 cm^{-1} band is in fact the shifted *d*-OH band. This conclusion is supported by "N_2O-ASW" spectra that are presented below, in which the absence of N_2O combination bands in this spectral region simplifies the spectrum.

N_2O Interactions with ASW Films. The experimental results obtained for N_2O and CO_2 are similar. The nature of the observed N_2O ν_3 features after dosing N_2O onto ASW films at 90 K depended on both the amount of N_2O dosed and the ASW film thickness. At low N_2O coverages, only a single band at 2215−2250 cm^{-1} was present (Figure 8). Two additional peaks at 2238 and 2256 cm^{-1} were evident at higher coverage. At 90 K, depositing equal amounts of N_2O onto ASW films that differ only in thickness demonstrated that the thinner the ASW film the greater the intensity of the 2238 and 2256 cm^{-1} features and the smaller the intensity of the 2215−2250 cm^{-1} band (Figure 9).

Isothermal desorption of the accumulated N_2O (deposited onto an ASW film at 90 K) for 15−20 min resulted in a "residual" N_2O band at 2222 cm^{-1} (Figure 10). A desorption temperature of 105 K was chosen because experiments involving N_2O films on water-free MgO substrates revealed that any N_2O deposited at 90 K desorbed before a substrate temperature of 100 K could be attained. Thus, spectra recorded in these experiments are due to N_2O that is present in the film, rather than on its surface. Figure 10 shows the sensitivity of this residual N_2O feature to ASW thickness. For an ASW film of a specific thickness, doubling the amount of N_2O dosed onto the film at 90 K did not necessarily double the intensity of the spectral feature associated with the remaining N_2O (Figure 11). A similar effect was seen with CO_2 (Figure 5).

The N_2O residual feature was stable at temperatures below the ice transition temperature. As shown in Figure 12, this IR band persisted even at a temperature of 155 K, which is much higher than the desorption temperature of pure N_2O films and only a few degrees below the ASW-to-crystalline transition temperature. Converting the ASW film to crystalline ice prior to 90 K N_2O adsorption results in no remaining N_2O features after 105 K isothermal desorption.

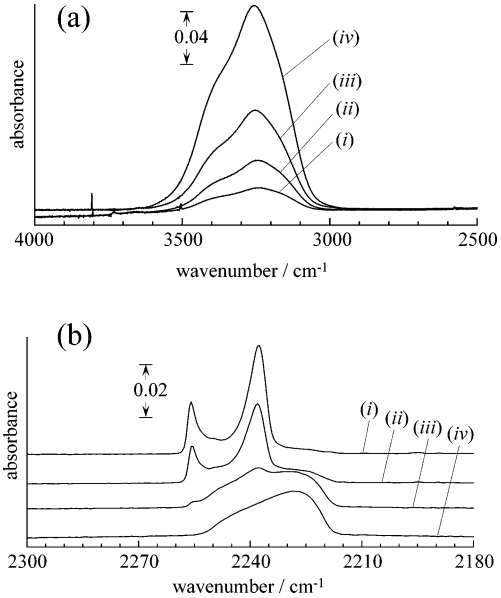

Figure 9. Spectra recorded with p-polarization. ASW films of different thicknesses were prepared at 90 K by exposure to H_2O at 4×10^{-8} Torr. (a) H_2O spectra labeled (i)−(iv) were recorded with exposures of (i) 4 min (∼15 layers), (ii) 8 min (∼35 layers), (iii) 16 min (∼70 layers), and (iv) 32 min (∼150 layers). (b) The corresponding N_2O spectra are labeled (i)−(iv). In all cases, N_2O exposure was 4×10^{-8} Torr for 4 min.

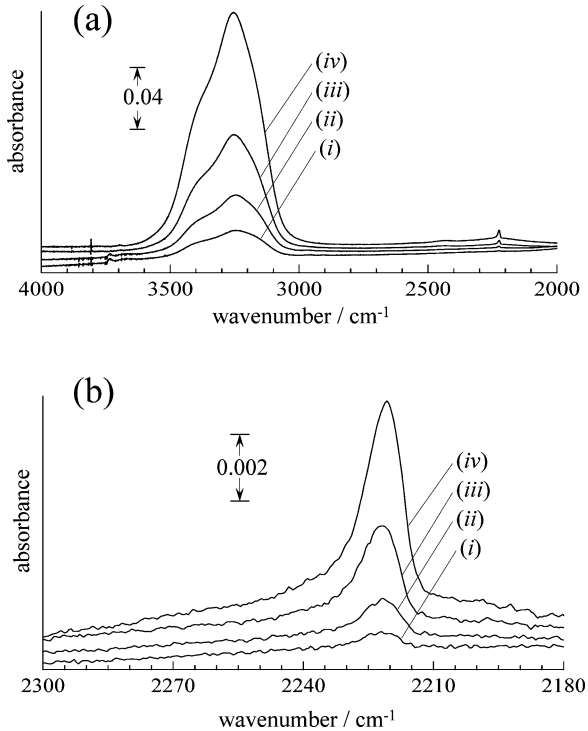

Figure 10. Spectra recorded with p-polarization. ASW films were exposed to N_2O (4×10^{-8} Torr for 4 min) at 90 K. The temperature was then raised to 105 K and kept there for 15−20 min before a spectrum was recorded (at 105 K). Approximate ASW thicknesses for (i)−(iv) were 15, 35, 70, and 150 layers, respectively. Entries (a) and (b) show H_2O and N_2O features, respectively.

ASW films formed on top of deposited N_2O led to residual N_2O intensities, after isothermal desorption, larger than those for ASW films situated beneath accumulated N_2O. In a series of experiments, N_2O was sandwiched between two ASW films at 90 K, and, aside from the amounts of water dosed prior to and after N_2O deposition, all variables (i.e., total amount of water and N_2O dosed, deposition and desorption temperatures) were the same in each experiment. All that changed was the respective thicknesses of the lower and upper ASW films. The constancy in the amount of total water is confirmed by the similarity in shape and intensity of the water IR band (Figure 13). As shown in Figure 13, the amount of N_2O remaining after 105 K desorption increased with increasing thickness of the top ASW film in these sandwiching experiments. The N_2O films deposited at 90 K create a rough interface between the ASW films where

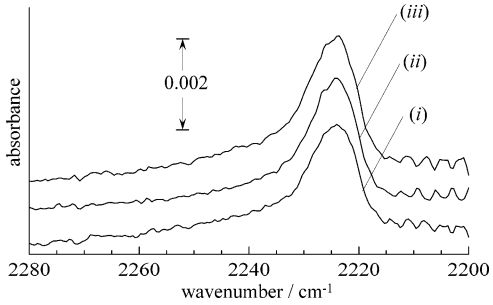

Figure 11. Spectra recorded with p-polarization of the N_2O that remained after depositing at 90 K different amounts of N_2O onto ASW films of constant thickness (∼70 layers) and then increasing the temperature to 105 K. The spectra were recorded at 105 K, 15−20 min after the temperature reached 105 K. N_2O exposure times at 4×10^{-8} Torr for (i)−(iii) were 2, 4, and 8 min, respectively. See Figure 8 for spectra recorded following N_2O deposition at 90 K.

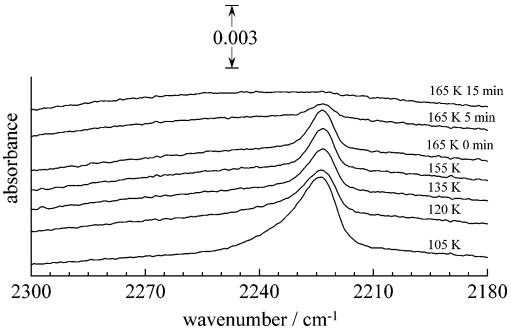

Figure 12. N_2O was deposited (4×10^{-8} Torr for 4 min) onto a 90 K ASW film of 40 layers. The temperature was then raised to 105 K and held there for 15 min, at which time a spectrum was recorded. The figure depicts the evolution of the spectra as the temperature was increased in steps to those shown and held at these temperatures for the duration of a scan (∼8 min). The spectra were recorded after each temperature increase and at the temperatures indicated. Three scans (∼5 min in duration) were recorded at 165 K; the time interval between reaching 165 K and commencing each of these scans is specified for the three relevant spectra.

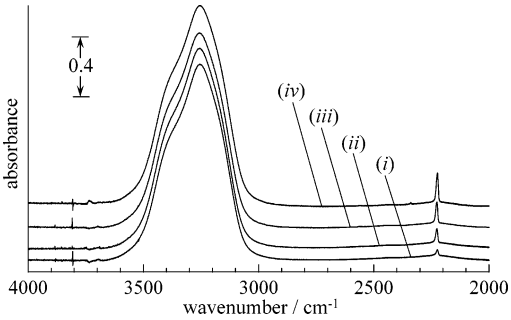

Figure 13. Spectra were recorded after sandwiching N_2O between two ASW films at 90 K, then raising the temperature to 105 K, and keeping it there for 15 min. The amount of deposited N_2O and the total number of water layers (∼80) is the same for all spectra. The ratios of bottom layer thickness to top layer thickness are (i) 80:0, (ii) 60:20, (iii) 40:40, and (iv) 20:60.

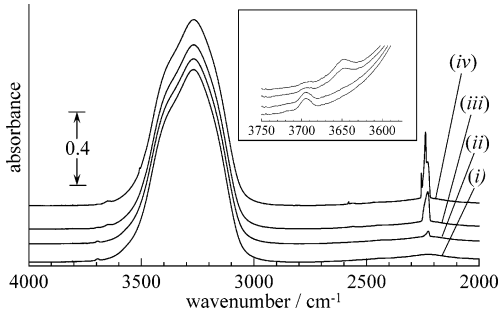

Figure 14. Spectra were recorded for different amounts of N_2O deposited onto an ASW film of ~1000 layers at 90 K. The amount of N_2O was increased via the sequence (i) no deposition, (ii) 4×10^{-8} Torr for 4 min, (iii) 1×10^{-7} Torr for 3 min, and (iv) 2×10^{-7} Torr for 7 min. Spectra were recorded immediately following each deposition. The inset shows that the *d*-OH feature is red shifted as a consequence of N_2O deposition; namely, the small *d*-OH humplet at ~3700 cm^{-1} moves to ~3650 cm^{-1}.

N_2O can reside at 105 K. Figure 13 can be reconciled by noting: (i) ASW films grown on N_2O overlayers are likely to be more porous than ASW films grown on MgO(100), where there is good registry and (ii) at 105 K, ASW films undergo some degree of annealing, which can trap dopant molecules.

The influence of N_2O on the position of the *d*-H peak is shown in Figure 14. As mentioned earlier, experiments monitoring the *d*-OH band focused on thick ASW films (>800 layers) because this band was hard to detect in thin ASW films. The spectra presented in Figure 14 were taken between successive doses of N_2O and they reveal a *d*-OH red shift of ~50 cm^{-1} as the amount of N_2O accumulates. Also, though some N_2O remains after isothermal desorption at 105 K, the *d*-OH peak returns to its original position at ~3700 cm^{-1}.

4. Discussion

When molecules are deposited on ice films, an issue to be addressed is where they reside after deposition. We shall consider three simple scenarios. One is that the molecules diffuse through the film and accumulate on the substrate via the displacement of water molecules. A second scenario involves molecules penetrating into the bulk of the ice and residing there. Localization on top of the water film surface is yet another possibility. Nothing precludes a priori the simultaneous participation of these processes.

The displacement of water molecules in the first adlayer (i.e., the layer in contact with the MgO substrate) by CO_2 is unlikely. Theoretical studies predict that the heat of adsorption of CO_2 on MgO(100) is $\Delta H_{ad} \sim 0.3$ eV.[27] In sharp contrast, the experimentally determined value of ΔH_{ad} for monolayer water on MgO(100) is ~0.8 eV, which is large for a physisorbed molecule.[24] It is this considerable difference in the ΔH_{ad} values that makes the displacement of monolayer H_2O by CO_2 improbable on this surface. It is assumed that this argument also applies to N_2O, despite the lack of theoretical or experimental binding energies for N_2O on MgO(100).

The two IR peaks at 2379 and 2345 cm^{-1} that emerge as CO_2 coverage increases (Figure 2) lie at energies that are similar to those of the LO and TO resonances of thin, polycrystalline CO_2 films.[26] These peaks also exhibit the same polarization dependence as the aforementioned resonances, i.e., the peak at ~2380 cm^{-1} is drastically reduced in spectra recorded with s-polarized light. Moreover, the $^{13}CO_2$ band at 2284 cm^{-1} that emerges as the exposure time of CO_2 to an ASW film increases, also appears in the spectra of CO_2 thin films. There is little doubt that these observations imply the formation of a CO_2 thin film. Similarly, the two additional IR features that grow in as N_2O accumulates (Figure 8) are correlated strongly with the LO and TO vibrational resonances of N_2O thin films.[26] The propensity of CO_2 and N_2O dosed onto ASW films at 90 K to produce features characteristic of polycrystalline CO_2 and N_2O indicates that enough accumulation of these molecules has occurred on top of the ASW film to yield thin films.

Some CO_2 and N_2O molecules enter the film interior even at 90 K. It is intuitive to assume that a property that varies with film thickness must be related to a phenomenon occurring in the interior. Consequently, it is easy to understand why the dependence of the CO_2 and N_2O band shapes on ASW thickness (Figures 3 and 9) leads us to conclude that some of these molecules diffuse into the film at 90 K. Both CO_2 and N_2O are expected to possess significant surface mobility because 90 K is only ~15 K lower than the temperature required for appreciable desorption. This mobility facilitates diffusion of small molecules into films.[28]

Prior to the formation of a CO_2 or N_2O thin film, the deposited molecules diffuse into and reside within the ASW film at 90 K. Also, the amount of favorable residence sites within ASW films rises as the film thickness grows. These conclusions originate primarily from the fact that film formation is only evident after a certain amount of CO_2 or N_2O has *already* accumulated. The relatively broad feature initially observed upon dosing these molecules onto ASW films (Figures 2 and 8) serves as evidence of this prior accumulation. This initial feature is assigned to probe molecules within the ASW film. Moreover, the integrated area of this band just prior to the emergence of the narrow LO and TO resonances scales linearly with film thickness over 2 orders of magnitude (10−1000 ASW layers). The possibility that CO_2 or N_2O molecules are all situated entirely on top of the ASW film and that the apparent influence of film thickness on probe molecule spectra is simply a manifestation of a change in ASW film surface roughness with film thickness is thus eliminated. This is because a surface roughening effect is not expected to maintain a linear relationship with film thickness over such a large range.

The conclusions stated above are consistent with the results depicted in Figures 2 and 8 where the increases in the LO and TO peak intensities can be correlated with an increase in CO_2 or N_2O film thickness. Specifically, the thinner the ASW film, the less the number of deposited molecules that are needed to fill the favorable sites within the ice film before CO_2 or N_2O thin film formation commences on the "populated" ice film (Figures 3 and 9).

The last statement addresses the issue introduced at the beginning of this section. Namely, where do the deposited molecules reside? Of the three scenarios under consideration, only the latter two are active in the systems under study here. Moreover, the experimental results were able to distinguish between probe molecule uptake into the bulk versus film formation.

Studies of the adsorption of small molecules often differentiate between monolayer (2D) and multilayer (3D) spectral features.[29−32] In these studies, interaction with the surface affects the energy levels of first-layer adsorbates in a manner that is distinct from the ensuing layers. This leads to monolayer IR signatures (at vibrational energies that differ from those of the multilayer) that saturate because of the finite number of adsorption sites. In addition, many of these investigations observe that the vapor pressure of the overlayers is at least 1 order of magnitude greater than that of the monolayer. Thus,

there is a temperature range in which isothermal desorption removes the multilayer but little of the monolayer.

Neither CO_2 nor N_2O displayed an isothermal desorption temperature that facilitated a distinction between monolayer and multilayer IR features of these molecules. Here, the term monolayer refers to the first layer of CO_2 or N_2O atop on the ASW film surface. For example, isothermal desorption of CO_2 deposited onto ASW resulted in a decrease in the CO_2 band intensity until either no CO_2 signature or only the residual CO_2 feature peaked $\sim$2340 cm^{-1} remained; the outcome depended upon the ASW film thickness. The fact that the residual 2340 cm^{-1} peak scales with film thickness indicates that it is not the monolayer band. IR features associated with the monolayer probably coincide with features of the multilayer. Furthermore, such a similarity in the peak positions and desorption temperatures of the monolayer and multilayer support the assumption that the binding energies of molecules in these two regimes are approximately the same. Martin et al.[33] found the difference in adsorption energies between monolayer and multilayer CO adsorbed on ASW to be $<$3 kJ/mol.

The fact that residual band integrated absorbance varies linearly with ASW film thickness suggests that this feature originates from CO_2 and N_2O within the film. Devlin noted that spectra of small molecules and water vapor co-deposited at temperatures $\sim$10 K are similar to spectra of molecules absorbed in ASW films.[28] Indeed, FTIR studies of CO_2-H_2O ices,[17] formed at 10 K and warmed to temperatures above 100 K demonstrate that these mixtures have a band at 2340 cm^{-1}. The substantial release of trapped molecules during the phase transition of ASW has been observed in previous studies.[27,34] Because this occurs as the film crystallizes, it depends on the experimental conditions that influence crystallization, e.g., heating rate and annealing temperature. In monitoring the main ASW band and the remaining CO_2 and N_2O IR signatures, it is clear that the release of any trapped molecules occurs during the conversion from ASW to cubic ice (see Figure 6).

A plausible process by which gases are trapped has been discussed by Ayotte et al.[27] They suggest that some of the molecules deposited onto the ASW film enter pores that open to the vacuum, and two things happen simultaneously when the film temperature is raised. The desorption rate of molecules accumulated within these pores rises, due to the temperature increase, whereas the ASW film undergoes a slight molecular rearrangement. This rearrangement closes avenues of connectivity to the vacuum possessed by some pores and, thus, traps molecules that have yet to desorb from the film interior. These trapped molecules remain enclosed in the film until ASW crystallization when the rearrangement required for the phase transition allows these molecules to escape.

The apparent saturation in the integrated absorbance of the residual band intensity for a specific ASW film (Figures 5 and 11) can be accounted for with such a model. Once the favorable sites within the film become populated, additional molecules localize on the film surface. If CO_2 and N_2O film formation does not drastically influence the desorption rate of molecules residing within the ASW, then isothermal desorption at a specific temperature will result in the trapping of approximately the same amount of molecules when *all* interior sites are populated. The assumption that both the desorption rate from ASW cavities and the rate of ASW film pore closure depend on temperature forms the basis of this inference. As stated earlier, the inability to calibrate CO_2 and N_2O coverage via TPD precluded a determination of CO_2 and N_2O concentrations from integrated absorbances. However, an estimate of 100 H_2O molecules for each trapped CO_2 molecule was obtained by using the integrated absorption cross section per molecule of the CO_2 ν_3 stretch in CO_2 films,[35] and assuming an ASW density and layer thickness of 0.9 g/cm^3 and 4 Å, respectively.

There is evidence of structural rearrangement in ASW films induced by annealing at temperatures well below that of the amorphous to cubic ice transition. Manca et al.[36] reported ASW reorganization commencing at 105 K, and Kimmel et al.[3] demonstrated that the thermal history of an ASW film influences its porosity. It was anticipated that these structural changes would lead to a decrease in the amount of trapped CO_2 and N_2O. To verify this, ASW films were annealed to 110−130 K for 15 min and then cooled to 90 K prior to CO_2 or N_2O deposition. The CO_2 and N_2O that remained after isothermal desorption was far less than the amount trapped by films that were not annealed in this manner. Thus, the 110−130 K annealing of ASW films deposited at 90 K results in structural rearrangements that influence the trapping of small molecules. It is noteworthy that this happens even though the ASW spectral signature undergoes no discernible change. Presumably these rearrangements are associated with collapsing pores that are responsible for trapping molecules. As mentioned earlier, crystalline films failed to trap a detectable amount of deposited molecules, consistent with the fact that these films lack significant porosity.

The presence of CO_2 and N_2O within the ASW film does not necessarily bring about a shift in the *d*-OH feature. As Figure 14 shows, this band remains unaffected by relatively small N_2O accumulations within the film. However, increasing the amount of deposited N_2O eventually leads to a 50 cm^{-1} red shift in the *d*-OH peak position.

Brunnauer−Emmet−Teller (BET) isotherms have been used to determine adsorption energies of molecules interacting with ice films.[33] These studies report no correlation between *d*-OH band shifts and heats of adsorption. Though no inferences are made here about interactions between ice and CO_2 or N_2O, recent theoretical efforts have been directed at determining parameters responsible for shifts of the *d*-OH group.[19] Thus, the data presented here provide grist for the mill of theory.

5. Summary

The experimental study described in this paper has explored issues of porosity, uptake, and transport in ASW films. The probe molecules CO_2 and N_2O provide IR spectral signatures that enable us to distinguish their surface films from their bulk inclusions in ASW hosts, including nuances such as binding to dangling OH sites. Good sensitivity is achieved because CO_2 and N_2O have strong ν_3 absorptions and relatively narrow spectral features, e.g., compared to those of the ASW host. This has enabled us to draw the conclusions listed below. These constitute a qualitative understanding of the associated phenomena.

(1) The ASW films grown at 90 K are porous. The CO_2 and N_2O guest molecules move throughout the bulk until essentially all of the adsorption sites are occupied.

(2) When the temperature of an ASW film is increased from its starting temperature of 90 K to temperatures in the range 110−130 K, the porosity changes dramatically. If the sample thus annealed is then cooled to 90 K, it can take up only about a third as much CO_2 or N_2O as freshly grown 90 K samples, i.e., samples that have not been annealed. It is interesting that this annealing brings about no discernible change in the ASW spectral feature centered at $\sim$3250 cm^{-1}.

(3) Some guest molecules within ASW films remain there as the temperature is increased from 90 to 155 K. Thereafter, the ASW to cubic ice transition occurs and these guest molecules are expelled. Once the ice film is crystalline, it is no longer possible for it to take up guest molecules within the film.

(4) Large inclusion regions can be prepared by using sandwiched films at 90 K: ASW−guest−ASW−guest− and so forth. Raising the temperature to 105 K drives off most of the guest molecules, though guest molecules are left behind that are included in the bulk. These display the same spectral signature as guest molecules that enter via transport from the surface into the bulk.

(5) Dangling OH bonds can be detected. Their spectral feature is sharp relative to that of the ASW film, as they are not hydrogen bonded. Guest molecules interact with these sites, resulting in a 50 cm^{-1} red shift. This is reminiscent of gas-phase studies of hydrogen-bonded dimers, where such effects are common.

Finally, we point out that the results presented here have a great deal in common with experimental studies that have been carried out using much larger ice thicknesses and mass spectroscopic diagnostics.[34,37,38] This work was brought to our attention by the reviewer, to whom we are grateful. The focus of these studies was astrophysical: properties of ices in comets, interstellar clouds, etc. Whereas our work has focused primarily on thicknesses <10 nm, the astrophysical studies have used sample thicknesses of at least several micrometers. Results obtained in these vastly different regimes are in qualitative accord where comparisons are appropriate. Some phenomena that are present with thick samples are absent with the relatively thin samples used here, e.g., plumes in which significant amounts of water are ejected. Most importantly, it will be of scientific interest to examine the intermediate regime, in which guest−host interactions can be traced from environments of a few tens of monolayers to macroscopic thicknesses.

References and Notes

(1) Jenniskens, P.; Blake, D. F. *Science* **1994**, *265*, 753.
(2) Stevenson, K. P.; Kimmel, G. A.; Dohnalek, Z.; Smith, R. S.; Kay, B. D. *Science* **1999**, *283*, 1505.
(3) Kimmel, G. A.; Stevenson, K. P.; Dohnalek, Z.; Smith, R. S.; Kay, B. D. *J. Chem. Phys.* **2001**, *114*, 5284.
(4) Pletzer, R.; Meyer, E. *J. Chem. Phys.* **1989**, *90*, 5207.
(5) Manca, C.; Martin, C.; Roubin, P. *Chem. Phys. Lett.* **2002**, *364*, 220.
(6) Smith, R. S.; Kay, B. D. *Surf. Rev. Lett.* **1997**, *4*, 781.
(7) Hagen, W.; Tielens, A. G. G. M.; Greenberg, J. M. *Chem. Phys.* **1981**, *56*, 367.
(8) Hudson, R. L.; Donn, B. *Icarus* **1991**, *94*, 326.
(9) Givan, A.; Loewenshuss, A.; Nielson, C. J. *J. Phys. Chem. B* **1997**, *101*, 8696.
(10) Schriver-Mazzuoli, L.; Schriver, A.; Hallou, A. *J. Mol. Struct.* **2000**, *554*, 289.
(11) Roland, B.; Devlin, J. P. *J. Chem. Phys.* **1991**, *94*, 812.
(12) Allouche, A.; Verlaque, P.; Pourcin, J. *J. Phys. Chem. B* **1998**, *102*, 89.
(13) Palumbo, M. E. *J. Phys. Chem. A* **1997**, *101*, 4298.
(14) Takoaka, T.; Inamura, M.; Yanagimachi, S.; Kusunoki, I.; Komeda, T. *J. Chem. Phys.* **2004**, *121*, 1 September 2004.
(15) Silva, S. C.; Devlin, J. P. *J. Phys. Chem.* **1994**, *98*, 10847.
(16) Buch, V.; Delzeit, L.; Blackledge, C.; Devlin, J. P. *J. Phys. Chem.* **1996**, *100*, 3732.
(17) Sandford, S. A.; Allamandola, L. J. *J. Astrophys.* **1990**, *355*, 357.
(18) Andersson, P. U.; Nagard, M. B.; Witt, G.; Pettersson, J. B. C. *J. Phys. Chem. A* **2004**, *108*, 4627.
(19) Manca, C.; Allouche, A. *J. Chem. Phys.* **2001**, *114*, 4226.
(20) Hawkins, S.; Kumi, G.; Malyk, S.; Reisler, H.; Wittig, C. *Chem. Phys. Lett.* **2004**, *404*, 19.
(21) Korolik, M.; Suchan, M. M.; Johnson, M. J.; Arnold, D. W.; Reisler, H.; Wittig, C. *Chem. Phys. Lett.* **2000**, *326*, 11.
(22) Xu, J.; Jansch, H. J.; Yates, J. T. *J. Vac. Sci. Technol.* **1993**, *A11*, 726.
(23) Somorjai, G. A. *Introduction to Surface Chemistry and Catalysis*; John Wiley and Sons: New York, 1994.
(24) Ferry, D.; Glebov, A.; Senz, V.; Suzzane, J.; Toennies, J. P.; Weiss, H. *J. Chem. Phys.* **1996**, *105*, 1697.
(25) Herzberg, G. *Infrared and Raman Spectra*; Van Nostrand Reinhold Co., Inc.: New York, 1945.
(26) Ovchinnikov, M. A.; Wight, C. A. *J. Chem. Phys.* **1993**, *99*, 3374.
(27) Ayotte, P.; Smith, R. S.; Stevenson, K. P.; Dohnalek, Z.; Kimmel, G. A.; Kay, B. D. *J. Geophys. Res.* **2001**, *106*, 33837.
(28) Devlin, J. P. *J. Phys. Chem.* **1992**, *96*, 6185.
(29) Heidberg, J.; Redlich, B. *Surf. Sci.* **1996**, *368*, 140.
(30) Heidberg, J.; Redlich, B.; Wetter, D. *Ber. Bunsen-Ges. Phys. Chem.* **1995**, *99*, 1333.
(31) Berg, O.; Ewing, G. E. *Surf. Sci.* **1989**, *220*, 207.
(32) Chang, H.; Richardson, H. H.; Ewing, G. E. *J. Chem. Phys.* **1988**, *89*, 7561.
(33) Martin, C.; Manca, C.; Roubin, P. *Surf. Sci.* **2002**, *502*−*503*, 275.
(34) Bar-Nun, A.; Dror, J.; Kochavi, E.; Laufer, D. *Phys. Rev. B* **1987**, *35*, 2427.
(35) Yamada, H.; Person, W. B. *J. Chem. Phys.* **1964**, *41*, 2478.
(36) Manca, C.; Martin, C.; Roubin, P. *Chem. Phys.* **2004**, *300*, 53.
(37) Bar-Nun, A.; Kleinfeld, I.; Kochavi, E. *Phys. Rev. B* **1988**, *38*, 7749.
(38) Bar-Nun, A.; Herman, G.; Laufer, D.; Rappaport, M. L. *Icarus* **1985**, *63*, 317.